Solar Cells

DOI: 10.1002/ange.201102552

Dye-Sensitized Solar Cells Based On Donor–Acceptor π-Conjugated Fluorescent Dyes with a Pyridine Ring as an Electron-Withdrawing Anchoring Group**

*Yousuke Ooyama, Shogo Inoue, Tomoya Nagano, Kohei Kushimoto, Joji Ohshita, Ichiro Imae, Kenji Komaguchi, and Yutaka Harima**

Since the first report of dye-sensitized solar cells (DSSCs) by Grätzel and co-workers in 1991,[1] DSSCs have received considerable attention because of their high incident solar light to electricity conversion efficiency and low cost of production. Recently, in order to increase power conversion efficiency, much research has focused on the development of new metal-free organic dye sensitizers.[2–9] In particular, donor–acceptor π-conjugated (D-π-A) dyes with both the electron-donating (D) and electron-accepting (A) groups linked by a π-conjugated bridge that exhibits broad and intense absorption, are proposed as one of the most promising organic dye sensitizers. The spectral features of the D-π-A dyes are associated with the intramolecular charge transfer (ICT) excitation from the donor to the acceptor moiety of the dye, thus leading to efficient electron transfer from the excited dye through the acceptor moiety into the conduction band (CB) of TiO_2. Most of the D-π-A dyes, such as coumarins, polyenes, thiophenes, and indolines, have dialkylamine or diphenylamine moieties as electron donor, and carboxylic acid, cyanoacrylic acid, or rhodanine-3-acetic acid moieties that act as electron acceptors as well as anchoring groups for attachment to a TiO_2 surface.[2–9] The carboxyl group enables good electronic communication between the dye and TiO_2 by forming a strong ester linkage with the TiO_2 surface. However, development of new D-π-A dyes for DSSCs is limited as long as the carboxyl group is employed as an anchor and electron acceptor. To create new and efficient D-π-A dyes for DSSCs, an new molecular design such as formation of a strong interaction between the electron-accepting moiety of sensitizers and TiO_2 surface is required.

Herein, we propose the use of a pyridine ring as an electron-withdrawing and anchoring group in place of a conventional carboxy group. We have demonstrated that the newly developed D-π-A fluorescent dyes NI**3**–**6** with a pyridine ring can adsorb onto a TiO_2 surface by strong coordinate bonding between the lone pair of electrons on the nitrogen atom of the pyridine, and the Lewis acid sites of TiO_2 to give electron injection efficiencies comparable to or higher than those for NI**1** and NI**2** where the pyridine ring is replaced with carboxyphenyl group (Scheme 1; see the Supporting Information for the detailed synthetic procedures).

The absorption and fluorescence spectra of NI**1**–**6** in 1,4-dioxane are shown in Figure 1 and their spectral data are

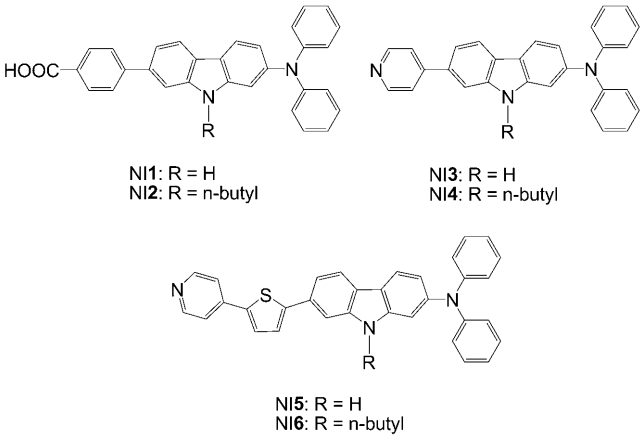

Scheme 1. Chemical structures of D-π-A fluorescent dyes NI**1**–**6**.

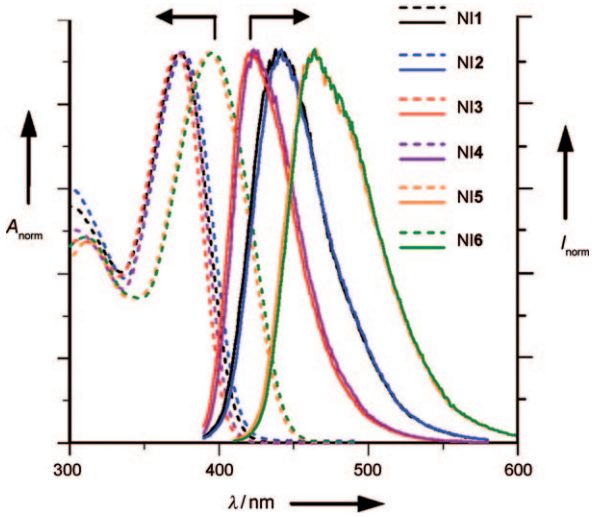

Figure 1. Absorption (-----) and fluorescence (——) spectra of NI**1**–**6** in 1,4-dioxane.

[*] Dr. Y. Ooyama, S. Inoue, T. Nagano, K. Kushimoto, Prof. Dr. J. Ohshita, Dr. I. Imae, Dr. K. Komaguchi, Prof. Dr. Y. Harima
Department of Applied Chemistry
Graduate School of Engineering, Hiroshima University
Higashi-Hiroshima 739-8527 (Japan)
E-mail: harima@mls.ias.hiroshima-u.ac.jp

[**] This work was supported by Grants-in-Aid for Young Scientists (B) (22750179) from the Japan Society for the Promotion of Science (JSPS).

Supporting information for this article is available on the WWW under http://dx.doi.org/10.1002/anie.201102552.

Table 1: Optical and electrochemical data, HOMO and LUMO energy levels, and DSSC performance parameters of NI**1**–**6**.

Dye	λ_{abs}[nm][a] (ε [$M^{-1}cm^{-1}$])	λ_{em} [nm][a] (Φ_F)	$E_{1/2}^{ox}$ [V][b]	HOMO [V][c]	LUMO [V][c]	Molecules/cm^2 [d]	J_{sc} [mA cm^{-2}][e]	V_{oc} [mV][e]	Fill factor[e]	η [%][e]
NI**1**	374 (34900)	438 (0.89)	0.30	0.93	−2.12	5.3×10^{16}	1.99	516	0.59	0.60
						10.4×10^{16}	2.96	503	0.61	0.91
NI**2**	376 (34300)	442 (0.87)	0.37	1.00	−2.03	4.8×10^{16}	1.80	517	0.60	0.56
						10.8×10^{16}	3.07	520	0.61	0.97
NI**3**	372 (30200)	423 (0.83)	0.34	0.97	−2.15	4.9×10^{16}	3.16	524	0.63	1.04
NI**4**	375 (33000)	423 (0.84)	0.39	1.02	−2.07	4.7×10^{16}	3.35	522	0.62	1.15
NI**5**	394 (48100)	465 (0.60)	0.30	0.93	−1.93	7.9×10^{16}	5.80	540	0.60	1.89
NI**6**	396 (49600)	464 (0.58)	0.34	0.97	−1.87	8.0×10^{16}	5.63	548	0.60	1.84

[a] In 1,4-dioxane. [b] Half-wave potentials for oxidation ($E_{1/2}^{ox}$) vs. Fc/Fc^+ were recorded in CH_2Cl_2/Bu_4NClO_4 (0.1 M) solution. [c] Potentials recorded vs. the NHE. [d] Adsorption amount per unit area of TiO_2 film was controlled by the immersion time of TiO_2 electrode in the dye solution. [e] The photocurrent–voltage characteristics were measured under a simulated solar light conditions (AM 1.5, 100 mW cm^{-2}).

summarized in Table 1. All the dyes show two absorption maxima: the band at around 300–315 nm is ascribed to a $\pi\rightarrow\pi^*$ transition, and the band at around 370–400 nm is assigned to the ICT excitation from the donor (diphenylamino group) to the acceptor (carboxyphenyl group for NI and NI**2** and pyridine ring for NI**3**–**6**). The ICT bands of NI**5** and NI**6** occur at a wavelength that is approximately 20 nm longer than those of NI**1**–**4**. Furthermore, the molar extinction coefficients (ε) for the ICT bands of NI**5** and NI**6** are approximately 50000 $M^{-1}cm^{-1}$ higher than the values of 30000–35000 $M^{-1}cm^{-1}$ for NI**1**–**4**. These results show that the introduction of thiophene unit onto the carbazole skeleton expands the π conjugation in the dye and thus results in the red-shift of absorption maximum and enhancement of the extinction coefficient. The corresponding fluorescence maximum (λ_{em}) occurs at around 420–465 nm. The fluorescent dyes NI**1**–**4** ($\Phi_F\approx0.85$) exhibit a higher fluorescence quantum yield Φ_F than those of NI**5** and NI**6** ($\Phi_F\approx0.6$).

Absorption spectra of the dyes adsorbed on TiO_2 nanoparticles are shown in Figure 2 (see the Supporting Information for details of the measurements). The absorption peak wavelengths (λ_{abs}) are red-shifted by approximately 10 nm for NI**1** and NI**2**, 25 nm for NI**3** and NI**4**, and 30 nm for NI**5** and NI**6** compared with those in 1,4-dioxane. Chenodeoxycholic acid (CDCA) has been employed as a coadsorbent to prevent dye aggregation on the TiO_2 surface. When CDCA is coadsorbed with NI**3**–**6** on TiO_2, the absorption peak wavelengths are blue-shifted by approximately 10 nm for NI**3** and NI**4** and 20 nm for NI**5** and NI**6**, although the peak wavelengths are still red-shifted compared with those in 1,4-dioxane. In contrast, the absorption peak wavelengths of NI**1** and NI**2** adsorbed on TiO_2 with coadsorption of CDCA are similar to those in 1,4-dioxane. These results show that the red-shifts of NI**3**–**6** adsorbed on TiO_2 are due to the strong interaction between the dyes and TiO_2 surface.

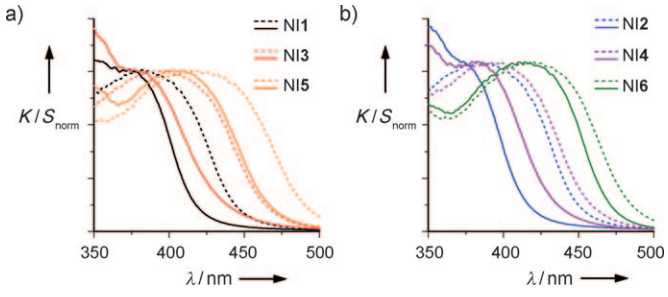

Figure 2. Absorption spectra of a) NI**1**, NI**3**, and NI**5** and b) NI**2**, NI**4**, and NI**6** adsorbed on TiO_2 nanoparticles with (——) and without (-----) CDCA as coadsorbent. The *y* axis is expressed in terms of the Kubelka–Munk equation $K/S=(1-R)^2/2R$, where *K* is the absorption coefficient, *S* is the scattering coefficient, and *R* is the fractional reflectance.

The electrochemical properties of all the dyes were determined by cyclic voltammetry (CV; see Figure S1 and Table S1 in the Supporting Information for the electrochemical properties). The oxidation peaks of NI**1**–**6** were observed at 0.34–0.42 V versus ferrocene/ferrocenium (Fc/Fc^+) and the corresponding reduction peaks appeared at 0.26–0.35 V, thus showing that the oxidized states of all the dyes are stable. The highest occupied molecular orbital (HOMO) and lowest unoccupied molecular orbital (LUMO) energy levels of all the dyes were evaluated from the spectral analyses and the half-wave potentials for oxidation of NI**1**–**6** ($E_{1/2}^{ox}=0.30$–0.39 V). The HOMO energy levels for NI**1**–**6** were 0.93–1.02 V versus the normal hydrogen electrode (NHE), thus indicating that all the dyes have similar HOMO energy levels that are more positive than the I_3^-/I^- redox potential (0.4 V). This property assures an efficient regeneration of the oxidized dyes by electron transfer from I^-/I_3^- redox couple in the electrolyte. The LUMO energy levels of the dyes were estimated from $E_{1/2}^{ox}$ and an intersection of absorption and fluorescence spectra (407 and 409 nm (3.05 and 3.03 eV) for NI**1** and NI**2**, 398 and 401 nm (3.12 and 3.09 eV) for NI**3** and NI**4**, and 434 and 436 nm (2.86 and 2.84 eV) for NI**5** and NI**6**), which correspond to the energy gap between the HOMO and the LUMO. The LUMO energy levels of NI**1**–**6** were −2.12, −2.03, −2.15, −2.07, −1.93, and −1.87 V, respectively. Evidently, these levels are higher than the energy level of the CB of TiO_2 (−0.5 V), so that these dyes can efficiently inject electrons to the TiO_2 electrode.

The MO calculations (AM1 and INDO/S)[10,11] showed that the absorption bands of these dyes were mainly assigned to the HOMO–LUMO transition, where HOMOs were mostly localized on the diphenylamino–carbazole moiety for NI**1**–**4** and the diphenylamino–thiophenyl–carbazole moiety for NI**5** and NI**6**, and LUMOs were mostly localized on the carboxyphenyl–carbazole moiety for NI**1** and NI**2**, the pyridinyl–carbazole moiety for NI**3** and NI**4**, and the pyr-

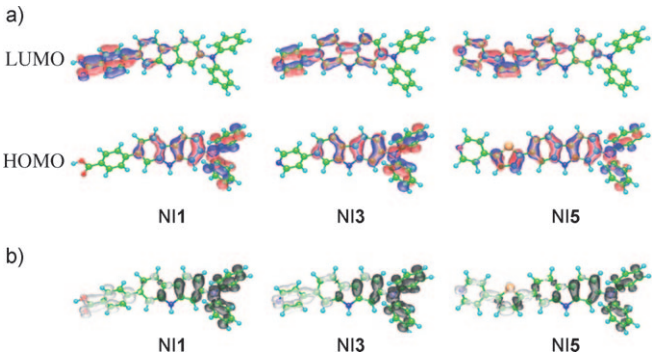

Figure 3. a) HOMO and LUMO of NI**1**, NI**3**, and NI**5**. The red and blue lobes denote the positive and negative phases of the coefficients of the molecular orbitals. The size of each lobe is proportional to the MO coefficient. b) Calculated electron density changes accompanying the first electronic excitation of NI**1**, NI**3**, and NI**5**. The black and white lobes signify decrease and increase in electron density accompanying the electronic transition, respectively. The areas indicate the magnitude of the electron density change. H light blue, C green, N blue, O red, and S gold.

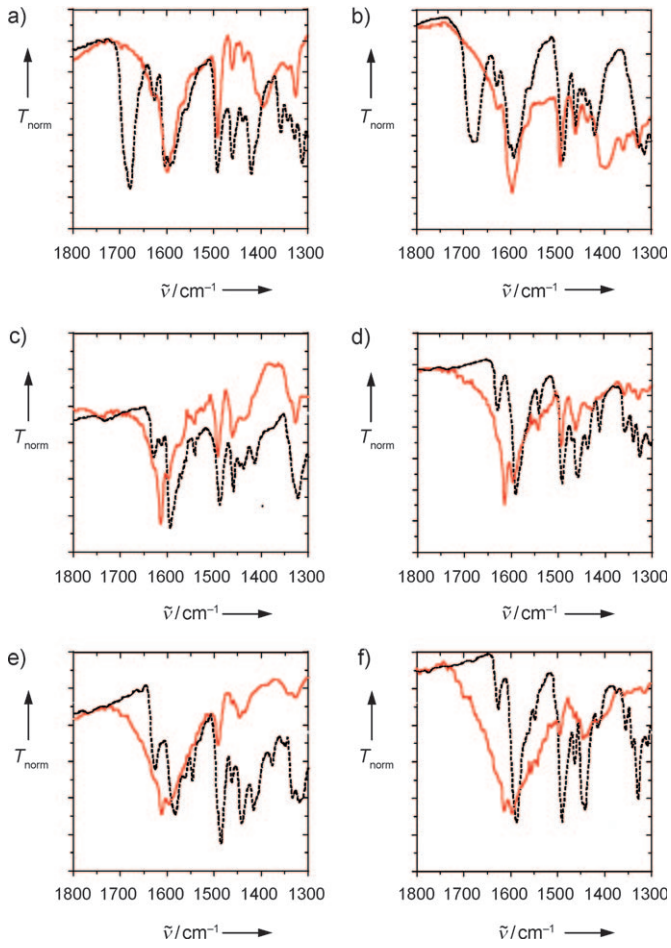

Figure 4. FTIR spectra of dye powders (-----) and dyes adsorbed on TiO_2 nanoparticles (——) for a) NI**1**, b) NI**2**, c) NI**3**, d) NI**4**, e) NI**5**, and f) NI**6**.

idinyl–thiophenyl–carbazole moiety for NI**5** and NI**6** (Figure 3a), thus suggesting a strong ICT nature upon irradiation (Figure 3b).

Figure 4 shows the FTIR spectra of the dye powders and the dyes adsorbed on TiO_2. For the powders of NI**1** and NI**2**, the C=O stretching band of carboxy group was observed at 1680 cm^{-1}. When the dyes were adsorbed on TiO_2 surface, the C=O stretching band at 1680 cm^{-1} disappeared. The observations indicate that the carboxy groups of the dyes form an ester linkage with TiO_2 surface.[12] On the other hand, the characteristic stretching bands for C=N or C=C were clearly observed at around 1590, 1490, and 1460 cm^{-1} for all the dye powders. In the FTIR spectra of NI**3–6** adsorbed on TiO_2, a new band appeared at around 1615 cm^{-1}, which is assigned to the pyridine ring coordinated to the Lewis acid sites of the TiO_2 surface.[13,14] This band indicates that the dyes NI**1** and NI**2** are adsorbed on the TiO_2 surface by the ester linkage alone at Brønsted acid sites (surface-bound hydroxy groups), whereas the dyes NI**3–6** are predominantly adsorbed on the TiO_2 surface by coordinate bonding at the Lewis acid sites (exposed Ti^{n+} cations). The strong coordinate bonding is responsible for the large red-shift of the absorption peak for NI**3–6** adsorbed on TiO_2 (Figure 2).

The DSSCs were prepared by using the dye-adsorbed TiO_2 electrode, platinum-coated glass as a counter electrode, and an solution of 0.05 M iodine, 0.1 M lithium iodide, and 0.6 M 1,2-dimethyl-3-propylimidazolium iodide in acetonitrile as electrolyte. The photocurrent–voltage (*I–V*) characteristics were measured under simulated solar light conditions (AM 1.5, 100 mW cm^{-2}). The *I–V* curves and the incident photon-to-current conversion efficiency (IPCE) spectra are shown in Figure 5. The photovoltaic performance parameters of DSSCs based on the dyes NI**1–6** are given in Table 1. The short-circuit photocurrent density (J_{sc}) and solar energy-to-electricity conversion yield (η, %) for NI**3** (3.16 mA cm^{-2}, 1.04%) and NI**4** (3.35 mA cm^{-2}, 1.15%) are similar to those for NI**1** (2.96 mA cm^{-2}, 0.91%) and NI**2** (3.07 mA cm^{-2}, 0.97%), when comparisons are made at maximum adsorption amounts of dyes adsorbed on TiO_2 (10.4×10^{16}, 10.8×10^{16}, 4.9×10^{16}, and 4.7×10^{16} molecules per cm^2 for NI**1**, NI**2**, NI**3**, and NI**4**, respectively) when using 1×10^{-4} M dye solutions in THF. The open-circuit photovoltages (V_{oc}) for NI**1–4** are 503 mV, 520 mV, 524 mV, and 552 mV, respectively, which were slightly different among the four dyes. The maximum IPCE values of NI**1–4** (47–55%) are in good agreement. Interestingly, when comparisons are made for similar amounts of dyes adsorbed on TiO_2 (5.3×10^{16}, 4.8×10^{16}, 4.9×10^{16}, and 4.7×10^{16} molecules cm^{-2} for NI**1**, NI**2**, NI**3**, and NI**4**, respectively), the J_{sc} and η values increase in the order of NI**2** (1.80 mA cm^{-2}, 0.56%) ≈ NI**1** (1.99 mA cm^{-2}, 0.60%) ≪ NI**3** (3.16 mA cm^{-2}, 1.04%) ≈ NI**4** (3.35 mA cm^{-2}, 1.15%). As shown in Figure 6, this result indicates that the formation of strong coordinate bonding between the pyridine ring of dyes NI**3** and NI**4** and the Lewis acid sites of the TiO_2 surface leads to an efficient electron injection owing to good electronic communication, rather than the formation of an ester linkage between the dyes NI**1** and **IN2** and the Brønsted acid sites of TiO_2 surface. However, the maximum amounts of dyes adsorbed on TiO_2 for NI**3** and NI**4** are about half the

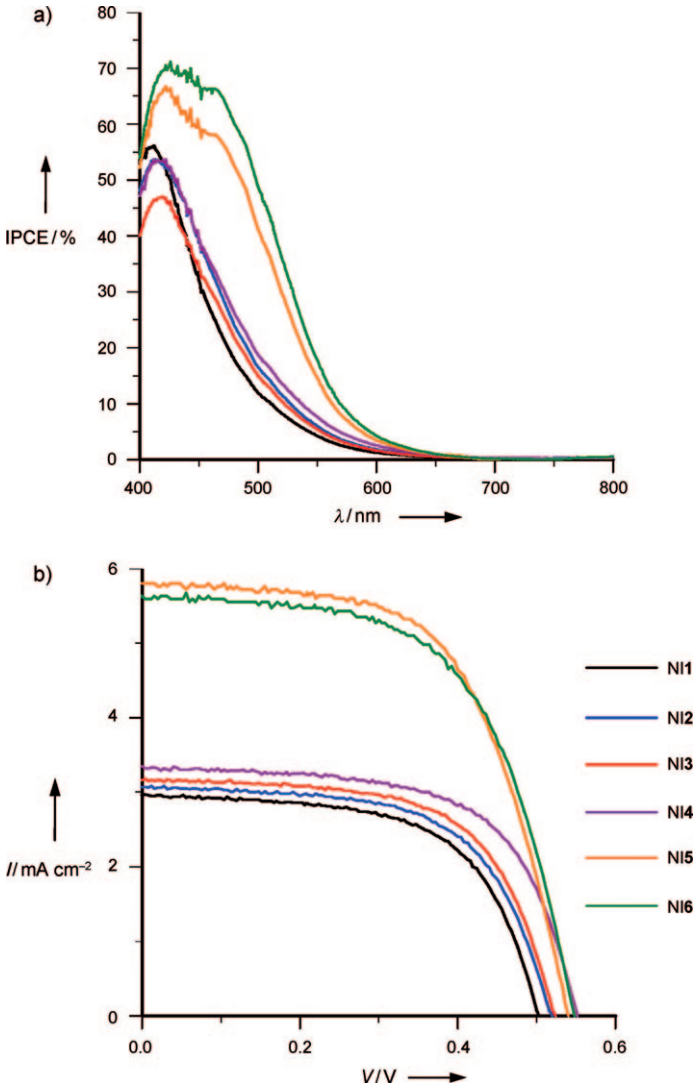

Figure 5. a) IPCE spectra and b) *I–V* curves of DSSCs based on NI**1**–**6**. The amounts of adsorbed dyes on TiO_2 film are 10.4×10^{16} (NI**1**), 10.8×10^{16} (NI**2**), 4.9×10^{16} (NI**3**), 4.7×10^{16} (NI**4**), 7.9×10^{16} (NI**5**), and 8.0×10^{16} molecules per cm^2 (NI**6**). 9 μm thick TiO_2 electrodes were used. CDCA was not employed. The same color code is used in (a) and (b).

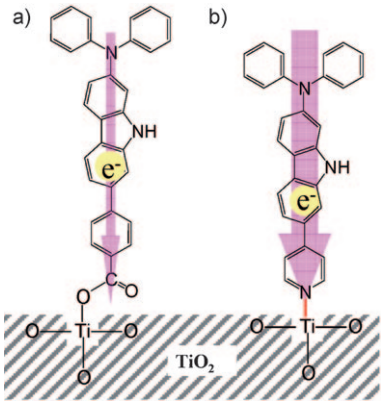

Figure 6. Configurations of a) NI**1** and b) NI**3** on the TiO_2 surface.

amounts of those for NI**1** and NI**2** because there are fewer Lewis acid sites on the TiO_2 surface than Brønsted acid sites. On the other hand, the J_{sc} and η values for NI**5** (5.80 mA cm^{-2}, 1.89%) and NI**6** (5.63 mA cm^{-2}, 1.84%) are larger than those for NI**3** and NI**4**. The maximum IPCE values of 65–70% for both NI**5** and NI**6** were observed in the range from 410 to 470 nm. The relatively high photovoltaic performances of NI**5** and NI**6** are attributed to both the red-shift of the absorption band and the good balance between the LUMO level of the dye and the energy level of the CB of TiO_2 by the introduction of a thiophene unit to the π-conjugation system of the dye. Thus, our results demonstrate that the dyes NI**3**–**5** can inject electrons efficiently from the pyridine ring as electron-withdrawing anchoring group to the CB of the TiO_2 electrode through the strong coordinate bonding with the Lewis acid site of the TiO_2 surface.

In conclusion, we have designed and synthesized fluorescent dyes NI**3**–NI**6** with a pyridine ring as electron-withdrawing anchoring group as new D-π-A dye sensitizers for DSSCs. We demonstrate that the formation of coordinate bonding between the pyridine ring of NI**3**–NI**6** and the Lewis acid sites of TiO_2 surface leads to an efficient electron injection arising from good electronic communication, rather than the formation of an ester linkage between NI**1** and NI**2** and the Brønsted acid sites of TiO_2 surface. Thus, we propose that the formation of a coordinate bond between the pyridine ring and the Lewis acid site of TiO_2 surface can be a promising candidate for electron-withdrawing anchoring group in new D-π-A dye sensitizers for DSSCs.

Received: April 13, 2011
Revised: May 30, 2011
Published online: June 29, 2011

Keywords: donor–acceptor systems · dyes/pigments · fluorescence · titanium dioxide · solar cells

[1] a) B. O'Regan, M. Grätzel, *Nature* **1991**, *353*, 737; b) A. Hagfeldt, M. Grätzel, *Chem. Rev.* **1995**, *95*, 49; c) U. Bach, D. Lupo, P. Comte, J. E. Moser, F. Weissörtel, J. Salbeck, H. Spreitzer, M. Grätzel, *Nature* **1998**, *395*, 583; d) M. Grätzel, *Nature* **2001**, *414*, 338.
[2] a) N. Robertson, *Angew. Chem.* **2006**, *118*, 2398; *Angew. Chem. Int. Ed.* **2006**, *45*, 2338; b) N. Robertson, *Angew. Chem.* **2008**, *120*, 1028; *Angew. Chem. Int. Ed.* **2008**, *47*, 1012.
[3] Z. Chen, F. Li, C. Huang, *Curr. Org. Chem.* **2007**, *11*, 1241.
[4] Z. Ning, H. Tian, *Chem. Commun.* **2009**, 5483.
[5] Y. Ooyama, Y. Harima, *Eur. J. Org. Chem.* **2009**, 2903.
[6] A. Mishra, M. K. R. Fischer, P. Bäuerle, *Angew. Chem.* **2009**, *121*, 2510; *Angew. Chem. Int. Ed.* **2009**, *48*, 2474.
[7] A. Hagfeldt, G. Boschloo, L. Sun, L. Kloo, H. Pettersson, *Chem. Rev.* **2010**, *110*, 6595.
[8] T. Bessho, S. M. Zakeeruddin, C.-Y. Yeh, E. W.-G. Diau, M. Grätzel, *Angew. Chem.* **2010**, *122*, 6796; *Angew. Chem. Int. Ed.* **2010**, *49*, 6646.
[9] H. Choi, I. Raabe, D. Kim, F. Teocoli, C. Kim, K. Song, J.-H. Yum, J. Ko, M. K. Nazeeruddin, M. Grätzel, *Chem. Eur. J.* **2010**, *16*, 1193.

[10] M. J. S. Dewar, E. G. Zoebisch, E. F. Healy, J. J. Stewart, *J. Am. Chem. Soc.* **1985**, *107*, 3902.
[11] a) J. E. Ridley, M. C. Zerner, *Theor. Chim. Acta* **1973**, *32*, 111; b) J. E. Ridley, M. C. Zerner, *Theor. Chim. Acta* **1976**, *42*, 223; c) A. D. Bacon, M. C. Zerner, *Theor. Chim. Acta* **1979**, *53*, 21; d) H. A. Kurtz, J. J. P. Stewart, D. M. Dieter, *J. Comput. Chem.* **1990**, *11*, 82.
[12] Z.-S. Wang, K. Hara, Y. Don-oh, C. Kasada, A. Shinpo, S. Suga, H. Arakawa, H. Sugihara, *J. Phys. Chem. B* **2005**, *109*, 3907.
[13] a) J. B. Peri, *Catalysis: Science and Technology*, *Vol. 5* (Eds.: J. R. Anderson, M. Boudart), Springer, Berlin, **1984**, pp. 171 – 220; b) A. A. Davydov in *Infrared Spectroscopy of Adsorbed Species on the Surface of Transition Metal Oxide*, (Ed.: C. H. Rochester), Wiley, Chichester, **1984**; c) M. W. Urban, *Vibrational Spectroscopy of Molecules and Macromolecules on Surfaces*, Wiley, Chichester, **1993**, pp. 171 – 185.
[14] a) M. I. Zaki, M. A. Hasan, F. A. Al-Sagheer, L. Pasupulety, *Colloids Surf. A* **2001**, *190*, 261; b) V. Vishwanathan, H.-S. Roh, J.-W. Kim, K.-W. Jun, *Catal. Lett.* **2004**, *96*, 23; c) M. M. Mohamed, W. A. Bayoumy, M. Khairy, M. A. Mousa, *Microporous Mesoporous Mater.* **2007**, *103*, 174.

